ORIGINAL ARTICLE

CANCER COMMUNICATIONS
Open Access

A novel intronic circular RNA, circGNG7, inhibits head and neck squamous cell carcinoma progression by blocking the phosphorylation of heat shock protein 27 at Ser78 and Ser82

Houyu Ju[1,2,3] | Zhenrong Hu[1,4] | Dongliang Wei[1,2,3] | Jinyun Huang[1,4] |
Xinyi Zhang[1,4] | Mengyu Rui[1,2,3] | Zhi Li[1,4] | Xiaomeng Zhang[3,5] |
Jingzhou Hu[1,2,3] | Wei Guo[1,2,3] 🄳 | Guoxin Ren[1,2,3] 🄳

[1] Department of Oral Maxillofacial-Head and Neck Oncology, Shanghai Ninth People's Hospital, Shanghai Jiao Tong University School of Medicine, Shanghai 200011, P. R. China

[2] Shanghai Key Laboratory of Stomatology & Shanghai Research Institute of Stomatology, National Clinical Research Center of Stomatology, Shanghai 200011, P. R. China

[3] National Clinical Research Center of Stomatology, Shanghai 200011, P. R. China

[4] School of Stomatology, Weifang Medical University, Weifang, Shandong 261053, P. R. China

[5] Shanghai Key Laboratory of Stomatology, Department of Oral and Maxillo-facial Implantology, School of Medicine, Shanghai Ninth People's Hospital, Shanghai Jiao Tong University, Shanghai 200011, P. R. China

Correspondence
Guoxin Ren, Jingzhou Hu, and Xiaomeng Zhang, Department of Oral and Maxillo-facial Surgery, Shanghai Ninth People's Hospital, Shanghai Jiao Tong University School of Medicine, Shanghai, 200011, P. R. China.
Email: renguoxincn@sina.com; huayayi@shsmu.edu.cn; zhangxiaomeng-wowo@126.com

Abstract

Background: There is increasing evidence that circular RNAs (circRNAs) play a significant role in pathological processes including tumorigenesis. In contrast to exonic circRNAs, which are the most frequently reported circRNAs in cancer so far, the studies of intronic circRNAs have been greatly lagged behind. Here, we aimed to investigate the regulatory role of intronic circRNAs in head and neck squamous cell carcinoma (HNSCC).

Methods: We conducted whole-transcriptome sequencing with four pairs of primary tumor tissues and adjacent normal tissues from HNSCC patients. Then, we characterized circGNG7 expression in HNSCC tissues and cell lines and explored

Abbreviations: circRNAs, circular RNAs; HNSCC, head and neck squamous cell carcinoma; SMAD4, SMAD family member 4; MAPK, mitogen-activated protein kinase; OS, overall survival; ceRNAs, competing endogenous RNAs; miRNAs, microRNAs; FISH, fluorescence in situ hybridization; HPV, Human Papilloma Virus; TNM stage, tumor, node, and metastasis stage; UICC, Union for International Cancer Control; STR, short tandem repeat; siRNAs, small interfering RNAs; WT, wild-type; qPCR, quantitative real-time polymerase chain reaction; GO, Gene Ontology; KEGG, Kyoto Encyclopedia of Genes and Genomes; GEO, Gene Expression Omnibus; RT-PCR, reverse transcription PCR; GAPDH, glyceraldehyde-3-phosphate dehydrogenase; SDS, sodium dodecyl sulfate; PVDF, polyvinylidene difluoride; IF, immunofluorescence; IHC, immunohistochemistry; CCK-8, Cell Counting Kit-8; EDU, 5-ethynyl-2'-deoxyuridine; sORF, open reading frame; EDTA, ethylene diamine tetraacetic acid; RIP, RNA immunoprecipitation; AGO2, Argonaute 2; TFs, transcription factors; ChIP, Chromatin immunoprecipitation; SPF, specific pathogen-free; PFS, progression-free survival; PI3K, phosphatidylinositol 3-kinase; HSP27, heat shock protein 27; GNG7, G protein subunit gamma 7; gDNA, genomic DNA; AZGP1, alpha-2-glycoprotein 1, zinc-binding; TGM3, transglutaminase 3; MAPKP38, mitogen-activated protein kinase P38; MAPK-APK-2, MAPK-activated protein kinase-2; PKD-1, polycystin 1; Mbl, Muscleblind; RSK2, p90 ribosomal S6 kinase 2; ERK5, signal-regulated kinase 5

its association with the prognosis of HNSCC patients. We also identified interactions between circGNG7 and functional proteins, which alter downstream signaling that regulate HNSCC progression.

Results: In this study, we identified a new intronic circRNA, circGNG7, and validated its functional roles in HNSCC progression. CircGNG7 was predominately localized to the cytoplasm, and its expression was downregulated in both HNSCC tissues andCAL27, CAL33, SCC4, SCC9, HN6, and HN30 cells. Low expression of circGNG7 was significantly correlated with poor prognosis in HNSCC patients. Consistent with this finding, overexpression of circGNG7 strongly inhibited tumor cell proliferation, colony formation, in vitro migration, and in vivo tumor growth. Mechanistically, the expression of circGNG7 in HNSCC cells was regulated by the transcription factor SMAD family member 4 (SMAD4). Importantly, we discovered that circGNG7 could bind to serine residues 78 and 82 of the functional heat shock protein 27 (HSP27), occupying its phosphorylation sites and hindering its phosphorylation, which reduced HSP27-JNK/P38 mitogen-activated protein kinase (MAPK) oncogenic signaling. Downregulation of circGNG7 expression in HNSCC increased HSP27-JNK/P38 MAPK signaling and promoted tumor progression.

Conclusions: Our results revealed that a new intronic circRNA, circGNG7, functions as a strong tumor suppressor and that circGNG7/HSP27-JNK/P38 MAPK signaling is a novel mechanism by which HNSCC progression can be controlled.

KEYWORDS

circGNG7, head and neck squamous cell carcinoma, heat shock protein 27 (HSP27), intronic circular RNAs, mitogen-activated protein kinase (MAPK) signaling, phosphorylation, tumor suppressor

1 | BACKGROUND

Head and neck squamous cell carcinoma (HNSCC), the dominant subtype of head and neck cancer, is the sixth most commonly diagnosed malignancy worldwide [1]. Although substantial advances have been made in recent decades, the prognosis of HNSCC remains poor [the 5-year overall survival (OS) rate was approximately 50%] due to local recurrence and regional lymphatic dissemination [2,3]. Hence, to improve clinical outcomes, a better understanding of the biological mechanisms underlying the tumorigenesis and progression of HNSCC is urgent.

Circular RNAs (circRNAs), a novel class of non-coding RNAs, have gained increasing attention due to their critical regulatory roles in tumorigenic processes [4]. CircRNAs are generated by a "backsplicing" event when a downstream pre-mRNA splice donor covalently links to an upstream splice acceptor [5]. CircRNAs appear to have higher stability than linear RNAs due to their inherent resistance to exonuclease activity [6]. Several biological functions have been assigned to circRNAs. CircRNAs may regulate the cellular physiology of cancer cells by acting as competing endogenous RNAs (ceRNAs), binding to functional proteins, or being directly translated into peptides or proteins [7]. CircRNAs also exhibit tissue-specific expression and exert particular functions in different types of cancer [8]. To date, several circRNAs, such as circPVT1 or circCORO1C, have been shown to exert vital effects on the progression and metastasis of HNSCC [9,10]. However, previous studies on HNSCC have mostly focused on the regulatory effects of circRNAs via their sponging of microRNAs (miRNAs) [11,12]. The interaction between circRNAs and their binding proteins has not been well elucidated in the context of HNSCC biology. Moreover, circRNAs can be classified as exonic circRNAs (derived from exons), exon-intron circRNAs (derived from both exons and introns), and intronic circRNAs (derived from intronic lariats) based on their origins Exonic circRNAs and exon-intron circRNAs are the most frequently reported, but the regulatory roles of intronic circRNAs in cancers have rarely been investigated.

Here, we performed whole-transcriptome sequencing on four pairs of primary tumor tissues and adjacent normal tissues from HNSCC patients to identify dysregulated intronic circRNAs and further investigated the biological function and underlying mechanism of an intronic circRNA, circGNG7, in HNSCC to provide new insight into HNSCC development.

2 | MATERIALS AND METHODS

2.1 | Clinical HNSCC specimens

A total of 69 HNSCC tissues were obtained from Shanghai Ninth People's Hospital Affiliated to Shanghai Jiao Tong University School of Medicine (Shanghai, China). Four pairs of tumor tissues (>2 cm^3) and adjacent normal tissues were randomly selected for whole-transcriptome sequencing analysis, and other 65 tissues were formalin-fixed and paraffin-embedded for fluorescence in situ hybridization (FISH) validation. These patients underwent their initial surgery between January 2016 and December 2017. Patients who were diagnosed as human papilloma virus (HPV)-positive, had local recurrences, or received preoperative chemo- or radiotherapy were excluded from our study. Our research was approved by the Ethics Board of the Shanghai Ninth People's Hospital, and informed consent was provided by the enrolled patients. The histological differentiation and tumor, node, and metastasis (TNM) stage were determined according to the criteria released by the Union for International Cancer Control (UICC, version 8.0) and World Health Organization Classification of Tumors (version 4.0), respectively [13].

2.2 | Cell culture

HNSCC cell lines SCC4, SCC9, CAL27, and CAL33 were purchased from Type Culture Collection of Chinese Academy of Sciences (Shanghai, China). HNSCC cell lines HN6 and HN30 were kind gifts from the University of Maryland (College Park, MD, USA). Normal oral keratinocytes were obtained and cultured from the gingival tissues of healthy volunteers. All these cell lines were verified by short tandem repeat (STR) genotyping before use. The cells were routinely cultured at 37°C in a standard humidified atmosphere containing 5% CO_2 in Dulbecco's modified Eagle medium (DMEM; Sigma, St. Louis, MO, USA) supplemented with 10% fetal bovine serum (Gibco, Grand Island, NY, USA), 100 μg/mL streptomycin sulfate and 100 U/mL penicillin sodium (Invitrogen, Carlsbad, CA, USA).

2.3 | Construction of small interfering RNAs (siRNAs), plasmids, and lentivirus and cell transfection

The overexpression plasmids (ov-circGNG7 and ov-HSP27), siRNA products (si-circGNG7 and si-HSP27), lentiviral vector overexpressing circGNG7 and the corresponding negative controls (vector and scramble) were synthesized by Genomeditech (Shanghai, China). In addition, plasmids expressing HSP27 with mutated serine phosphorylation sites (Ser15, Ser78, and Ser82) were purchased from GenScript (Piscataway, NJ, USA). The LASAGNA-Search 2.0 tool (https://biogrid-lasagna.engr.uconn.edu/lasagna_search/) was utilized to predict the binding sites between SMAD4 and the GNG7 promoter. The target site included 2000 bp (−2000 bp to 0 bp) upstream of the GNG7 promoter, and the binding site with the highest score and $P < 0.01$ was selected. The mutant sequence was designed based on the sequence of the predicted binding site. The wild-type (WT) and mutant promoter sequences were synthesized and inserted into the pGL3-Basic luciferase vector (Promega Cooperation, Madison, WI, USA) to generate plasmids carrying the WT and mutant GNG7 promoters. The sequences of ov-circGNG7, ov-HSP27, si-circGNG7, si-HSP27, HSP27-S15A, HSP27-S78A, and HSP27-S82A are shown in Supplementary Table S1. Lipofectamine™ 3000 (Invitrogen) was utilized to transfect the siRNAs and plasmids following the manufacturer's instructions. Functional experiments were conducted 24 h after transfection. The cells were infected with lentiviral vectors at a multiplicity of infection of 50 and cultured with 5 μg/mL puromycin (Invitrogen) for 2 weeks. The efficiency of siRNA transfection, plasmid transfection and lentiviral infection was verified by quantitative real-time polymerase chain reaction (qPCR) and Western blotting.

2.4 | Whole-transcriptome sequencing analysis

The total RNA was extracted with Trizol reagent (Invitrogen) from four pairs of tumor tissues and adjacent normal tissues of HNSCC patients and sent for whole-transcriptome sequencing analysis, including 49,200 circRNA probes and 20,308 mRNA probes (Cloudseq, Shanghai, China). Datasets and images were obtained by Agilent Feature Extraction software (version 11.0.1.1, Agilent Technologies, Santa Clara, CA, USA) following the manufacturer's instructions [14]. Dysregulated circRNA expression was considered significant at absolute fold change (FC) >2 and false discovery rate (FDR) <0.05. The

whole-transcriptome sequencing was performed by Cloud-seq Company. Gene Ontology (GO) and Kyoto Encyclopedia of Genes and Genomes (KEGG) pathway analysis were then performed. The enrichment score of dysregulated genes was calculated by the negative logarithm of P value. The significant GO term clusters and associated pathways were analyzed by using the calculated enrichment scores. The circRNA expression analysis results obtained during the current study are accessible through Gene Expression Omnibus (GEO) using the series accession number GSE159382 (https://www.ncbi.nlm.nih.gov/geo/query/acc.cgi?acc=GSE159382).

2.5 | Nuclear and cytoplasmic RNA isolation, reverse transcription PCR (RT-PCR), and qPCR

Total mRNA and circRNA were extracted with TRIzol reagent (Invitrogen). Cytoplasmic and nuclear circRNAs were isolated with an RNA Purification Kit (Norgen Biotek, Thorold, ON, Canada). Complementary DNA (cDNA) was reversely transcribed with a Prime Script RT reagent Kit (Takara, Dalian, Liaoning, China).

We constructed a pair of divergent primers and a pair of standard convergent primers to amplify circGNG7 and GNG7. RT-PCR assays were conducted with a SYBR Premix Ex Taq Reagent Kit (Takara), and the reaction condition was denatured at 95°C for 30 s, followed by 40 cycles of annealing/elongation at 95°C for 5 s and 60°C for 30 s. The datasets were analyzed using an ABI StepOne Real-Time PCR System (Thermo Fisher, Waltham, MA, USA). The $2^{-\Delta\Delta Ct}$ method was used to calculate the relative mRNA expression from the RT-PCR data. In addition, qPCR was performed to evaluate the absolute quantity of RNA following the standard method. The total and cytoplasmic RNA levels were normalized to glyceraldehyde-3-phosphate dehydrogenase (GAPDH). Small nuclear U6 was utilized for the normalization of nuclear RNA levels. The sequences of the primers we used are listed in Supplementary Table S1.

2.6 | Western blotting experiments

Western blotting experiments were conducted as we previously described [15]. Briefly, proteins were extracted with sodium dodecyl sulfate (SDS) lysis buffer (Beyotime, Shanghai, China) containing proteinase and phosphatase inhibitors (Roche Applied Science, Indianapolis, IN, USA). Then, the proteins were separated in 10% polyacrylamide gels and transferred to polyvinylidene difluoride (PVDF) membranes (Merck Millipore, Darmstadt,

Germany). After blocking with 5% bovine serum albumin and incubation with antibodies, the blotting bands were analyzed by an Odyssey Infrared Imaging System (Biosciences, Lincoln, NE, USA). GAPDH was utilized as the control protein, and the antibodies used are shown in Supplementary Table S2.

2.7 | Sanger sequencing

Total circRNA was extracted from CAL27 cells and reversely transcribed into cDNA. Then, the cDNA was amplified by qPCR with divergent primers. PCR amplification products were purified by Qiaquick Gel Extraction Kit (Qiagen, Hilden, Germany) and subjected to Quick Shot Sanger Sequencing by using Baseclear BV (Baseclear, Leiden, The Netherlands) to confirm the head-to-tail splicing of circGNG7.

2.8 | RNase R treatment and actinomycin D assay

Total RNA was extracted from CAL27 and HN6 cells and incubated with or without 20 U/μL RNase R (Geneseed Biotech, Guangzhou, Guangdong, China) at 37°C for 15 min, and the expression levels of circGNG7 and GNG7 were subsequently measured by RT-PCR. For the actinomycin D assay, CAL27 and HN6 cells were exposed to 2 μg/mL actinomycin D (Sigma) for the indicated time points. Then, circRNA and linear RNA were extracted and subjected to qPCR analysis.

2.9 | FISH, immunofluorescence (IF), immunohistochemistry (IHC), and RNAscope analysis

A probe targeting circGNG7 for RNAscope [16] was synthesized by Advanced Cell Diagnostics Company (Hayward, CA, USA), and a probe targeting circGNG7 for FISH was synthesized by RiboBio Company (Guangzhou, Guangdong, China). For FISH, CAL27 and HN6 cells were incubated with the indicated probe overnight at 4°C and imaged by confocal microscopy (Carl Zeiss Microscopy GmbH, Jena, Germany). 18S RNA and U6 were utilized to identify the cytoplasm and nucleus.

For RNAscope, the expression of circGNG7 in tissues from HNSCC patients was detected by a BaseScope™ Detection Reagent kit (Advanced Cell Diagnostics), and the data were subsequently analyzed using CaseViewer software (3D HISTECH, Budapest, Hungary). The signals were visually detected and could be classified into five

grades based on the following criteria: no staining or < 1 dot per 10 cells (grade 0), 1-3 dots per cell (grade 1), 4-9 dots per cell and no or very few dot clusters (grade 2), 10-15 dots per cell and < 10% of the dots existed in clusters (grade 3), and > 15 dots per cell and > 10% of the dots existed in clusters (grade 4). The circGNG7 expression level was defined as high when the RNAscope score was ≥ grade 2 and low when the RNAscope score was < grade 2.

IHC was conducted as we previously described [15]. Briefly, the specimens were deparaffinized using dimethylbenzene and alcohol (Sigma) with corresponding concentration gradient, rehydrated and subsequently washed by using phosphate buffered saline (PBS). After retrieving antigens by using citrate buffer (Sigma) for 30 min and blocking endogenous enzymes, the slides were incubated with corresponding antibodies. The slides were then stained and analyzed under microscope (Leica Microsystems, Wetzlar, Germany). The antibodies used are shown in Supplementary Table S2. The staining score was calculated as the product of the percentage of positive cells and the intensity of staining. The percentages of positive cells were classified based on the following criteria: less than 10% (grade 0), 10% to 25% (grade 1), 26% to 50% (grade 2), 51% to 74% (grade 3), and more than 75% (grade 4). The intensity of staining was scored according to the following criteria: no staining (score 0), bright yellow (score 1), orange (score 2), and brown (score 3). Total scores were calculated by multiplying the percentage of positive cells by the intensity of staining. Total scores of ≤1, 2–4, 5–8, and ≥9 indicated negative, low, moderate, and high expression, respectively.

For IF, CAL27 and HN6 cells were fixed by 4% paraformaldehyde (Sigma) for 15 min, permeabilized by 0.5% Triton X-100 (Sigma) for 20 min, blocked by goat serum (Sigma) for 30 min, and then incubated with the indicated primary antibodies overnight at 4°C. The samples were subsequently incubated with secondary fluorescently labelled antibodies for 30 min and incubated with 4',6-diamidino-2-phenylindole (DAPI; Invitrogen) at a dilution of 1:300. The slides were observed by using a confocal microscope.

2.10 | Cell viability, DNA synthesis, and colony formation experiments

CAL27 and HN6 cells transfected with overexpression plasmids or siRNAs targeting circGNG7 or HSP27 were seeded in 96-well plates. Cell Counting Kit-8 (CCK-8) assays (Dojindo Laboratories, Kumamoto, Japan) and 5-ethynyl-2'-deoxyuridine (EDU) assays (RiboBio) were performed following the manufacturers' protocols. CAL27 and HN6 cells were seeded in 6-well plates, incubated for 10 days, and then stained with crystal violet. The number of formed colonies was calculated to evaluate the colony forming capacity.

2.11 | Migration, invasion, and wound healing assays

Transwell assays were performed to analyze cell migration and invasion. Uncoated polycarbonate inserts (Millipore) were used for the migration experiment, and Bio-Coat™ inserts (BD Biosciences, Franklin Lake, NJ, USA) were used for the invasion experiment. Transfected CAL27 and HN6 cells were seeded in the upper chamber. After 24 h, the cells were stained with crystal violet, and the number of crystal violet-positive cells on the membrane was counted in three randomly selected fields of view at a magnification of 100×. For the wound healing assay, cells were seeded in 6-well plates, and a 20-μL pipette tip was utilized to scratch a uniform linear wound in the cell monolayer. Cell migration across the wound was observed at 0 h and 24 h after scraping, and fields of view were randomly selected and photographed.

2.12 | Biotinylated miRNA pull-down assay to identify miRNA targets

Biotinylated DNA probes against the fusion site of the circGNG7 (GenePharma Co., Shanghai, China) and the negative control primer were incubated with cell lysates of HN6 and CAL27 cells at 4°C overnight. Then, the biotinylated RNA complexes were pulled down, and certain RNAs were extracted from the input and pull-down beads by using TRIzol (Invitrogen) according to the manufacturer's instruction. The abundance of miRNAs in the bound fraction was detected by RT-PCR analysis.

2.13 | Prediction of the coding potential of circGNG7

The sequence of circGNG7 was obtained from the circBase database (http://www.circbase.org/). The coding potential of circGNG7 was predicted by assessing whether a small open reading frame (sORF) was present with a public web server named CNIT (http://cnit.noncode.org/CNIT) [17].

2.14 | RNA pull-down assay and proteomic analysis

RNA pull-down assays were conducted as previously described [18]. Biotinylated DNA probes complementary to the circRNA fusion site and a negative control primer were

used for the RNA pull-down assays. CAL27 cells transfected with circGNG7 and the HSP27, HSP27-S78A, and HSP27-S82A plasmids were fixed with 1% formaldehyde for 15 min. The fixation reaction was quenched by adding a 1/20 volume of 2.5 mol/L glycine and incubating the samples for 5 min at 25°C. The cells were resuspended in sonication buffer [20 mmol/L Tris-HCl (pH = 8.0), 2 mmol/L ethylene diamine tetraacetic acid (EDTA), 1% Triton X-100, 150 mmol/L NaCl, 1 mmol/L phenylmethylsulfonyl fluoride, 0.5% SDS] and sonicated with a Bioruptor® Pico sonication device (Diagenode, Liège, Belgium) for 5 cycles (30 s on/30 s off).

The hybridization of the biotinylated probes and the circRNA was conducted in hybridization buffer (50 mmol/L Tris-HCl pH 7.0, 750 mmol/L NaCl, 1 mmol/L EDTA, 1% SDS, 15% formamide). After 6 h of hybridization, the probe-circRNA complexes were captured by streptavidin-coated magnetic beads (#20164, Thermo Fisher Scientific) after washing five times in wash buffer (0.5% SDS, 2× SSC). The complexes were eluted with biotin elution buffer and subjected to proteomic analysis or Western blotting analysis. The proteomic analysis was performed with the Q Exactive™ Plus Orbitrap LC-MS/MS system (Thermo Fisher Scientific) in Shanghai DianXi Bio (Shanghai, China), and the proteins that were determined by proteomic analysis to be directly bound to circGNG7 are listed in Supplementary Table S3.

2.15 | RNA immunoprecipitation (RIP)-qPCR

The RIP experiment was conducted using the Magna RIP™ RNA-Binding Protein Immunoprecipitation Kit (17–700, Millipore) following the manufacturer's protocols. The primers specific for the circGNG7 fusion site and the linear sequence of the host gene are listed in Supplementary Table S1. qPCR analysis was performed using HiScript III RT SuperMix for qPCR (+gDNA wiper) (R323-01, Vazyme, Nanjing, Jiangsu, China) and ChamQ SYBR Color qPCR Master Mix (Q411-02, Vazyme) following the manufacturer's protocols. CAL27 cells were transfected with the miR-34c-5p mimic or control RNA, and Argonaute 2 (AGO2)-RIP assays were performed using the Magna RIP™ RNA-Binding Protein Immunoprecipitation Kit. CAL27 cells were lysed, and then the lysates were incubated with magnetic beads. The magnetic beads were conjugated to human anti-AGO2 antibodies or control mouse IgG. After incubation with proteinase K (Gibco), the immunoprecipitated RNAs were isolated and extracted. The enrichment of circGNG7 was determined by PCR analysis.

2.16 | Prediction of transcription factor-binding sites

LASAGNA-Search 2.0 (http://biogrid-lasagna.engr.uconn.edu/lasagna_search/) was adopted to predict possible transcription factors (TFs) that may bind to the promoter of GNG7.

2.17 | Dual-luciferase reporter assay

The promoter-luciferase construct and pRL-TK Renilla luciferase construct (GenePharma Co.) were cotransfected into CAL27 or HN6 cells. The luciferase activity was assessed with a Dual-Luciferase Reporter Assay kit (Beyotime) 48 h after transfection following on the manufacturer's protocol.

2.18 | Chromatin immunoprecipitation (ChIP) assay

293T or CAL27 cells were fixed, lysed, and sonicated to generate ∼500 bp fragments. The cell lysates were incubated with SMAD4 antibodies (1:50 dilution) overnight at 4°C. The precipitated mixture was washed, eluted, purified, and then examined by qPCR. The primer specific for the circGNG7 promoter was synthesized by Sangon Biotech (Shanghai, China), and the primer sequences are listed in Supplementary Table S1.

2.19 | Tumorigenesis and metastasis in vivo study

CAL27 cells transfected with lentiviral vectors overexpressing circGNG7 were subcutaneously injected into the flanks of BALB/c nude mice (purchased from Shanghai Laboratory Animal Center, Shanghai, China) to established a circGNG7-overexpressed xenograft model. The tumor volumes were gauged and calculated every 3 days using the following formula: volume (mm^3) = width^2 × length/2. The tumor weights were measured after the mice were euthanized by cervical vertebrae luxation 30 days after the model was established (tumor volume > 40 mm^3).

CAL27 cells stably overexpressing circGNG7 were injected into the tail vein to establish a lung metastasis model. After 8 weeks, the lungs were excised and fixed in Bouin's fixative diluted with neutral-buffered formalin at a ratio of 1:5, and then the lung colonization nodules were counted.

All the mice were bred under specific pathogen-free (SPF) conditions at Shanghai Laboratory Animal Center. All the experimental protocols were approved by the Animal Ethics Committee of Shanghai Ninth People's Hospital.

2.20 | Statistical analysis

The data were analyzed with SPSS software version 19.0 (SPSS Inc., Chicago, IL, USA). One-way analyses of variance (ANOVA) and Student's *t*-tests were utilized to assess the statistical significance. The Kaplan-Meier method was used to analyze the OS and progression-free survival (PFS) data. OS was defined as the time from disease diagnosis to death from any causes, and PFS was defined as the time from disease diagnosis to radiographically confirmed progression or death which ever occurred first. The clinical variables affecting prognosis were assessed by Cox proportional hazards regression analysis. $P < 0.05$ was considered to indicate statistical significance.

3 | RESULTS

3.1 | CircGNG7 expression was downregulated in HNSCC tissues and indicated poor prognosis in HNSCC patients

To investigate the roles of circRNAs in HNSCC, we conducted a whole-transcriptome sequencing analysis with four pairs of HNSCC tissues and their matched adjacent normal tissues (Supplementary Table S4). A total of 29 circRNAs (13 upregulated and 16 downregulated) and 2,185 mRNAs (1,078 upregulated and 1,107 downregulated) exhibited dysregulated expression in HNSCC (Supplementary Figure S1A and B). In our previous whole-transcriptome sequencing study of metastatic oral mucosal melanoma, we showed that circGNG7 expression was decreased in metastatic lymph nodes compared with non-metastatic lymph nodes and that circGNG7 expression was associated with poor prognosis [19]. However, we did not continue to further investigate circGNG7 expression in oral mucosal melanoma due to the lack of proper oral mucosal melanoma cell lines. In our HNSCC whole-transcriptome sequencing data, we again identified circGNG7, which was among the top five downregulated known circRNAs (Figure 1A, Supplementary Table S5). GO and KEGG pathway analysis suggested that circGNG7 might exert regulatory effects through several cancer-related genes and signaling pathways, such as the genes involving in signal transducer activity and heterotrimeric G-protein complex iden-

tified by GO analysis and the Ras signaling pathway, phosphatidylinositol 3-kinase (PI3K)-Akt signaling pathway, and chemokine signaling pathways identified by KEGG analysis (Supplementary Table S6). Thus, we focused on circGNG7 for further study.

We used RNAscope technology to investigate the relationship between the expression of circGNG7 and the clinical characteristics of HNSCC patients. It revealed that lower circGNG7 expression was associated with advanced T and N stage, while other clinical parameters showed no differences (Supplementary Table S7). We observed that circGNG7 was predominantly localized to the cytoplasm and was barely present in the nucleus of cells in tumor and adjacent normal tissues (Figure 1B). To examine the subcellular localization of circGNG7, we further performed PCR analysis and FISH assay to detect nuclear and cytoplasmic circGNG7 expression and found that circGNG7 was predominantly located in the cytoplasm and less appeared in the nucleus in both CAL27 and HN6 cells (Figure 1C and D). RNAscope analysis revealed that circGNG7 expression was reduced in tumor tissues compared with matched adjacent normal tissues from 65 patients (Figure 1E). Moreover, lower staining scores were associated with advanced UICC clinical stage, T stage, and N stage of HNSCC tissues (Figure 1F and G). Furthermore, lower staining scores were associated with lower OS rates and PFS rates (Figure 1H). Consistent with a previous study [20], the expression of G protein subunit gamma 7 (GNG7), the parental gene of circGNG7, was decreased in HNSCC patients, but its expression was not significantly associated with prognosis in HNSCC patients (Supplementary Figure S1C–E). Taken together, these data demonstrated that lower expression of circGNG7 might facilitate the progression of HNSCC and lead to poor outcomes for patients.

3.2 | Characteristics of circGNG7 expression in HNSCC

We next assessed circGNG7 expression in HNSCC cell lines. The expression of circGNG7 in five HNSCC cell lines (CAL27, CAL33, SCC4, SCC9, HN6, and HN30 cells) was lower than its expression in normal oral keratinocytes (Figure 2A). We selected CAL27 cells (with lowest circGNG7 expression) and HN6 cells (with highest circGNG7 expression) for subsequent experiments. Then, we analyzed the structure of circGNG7, which is derived from the fourth intron of its linear parental gene, GNG7, and has a length of 462 nt. The back-spliced junction sequence of circGNG7 was confirmed by Sanger sequencing, and the sequence was consistent with the annotation in the circBase database (Figure 2B). As shown in Figure 2B and Supplementary Figure S2, the divergent primers could
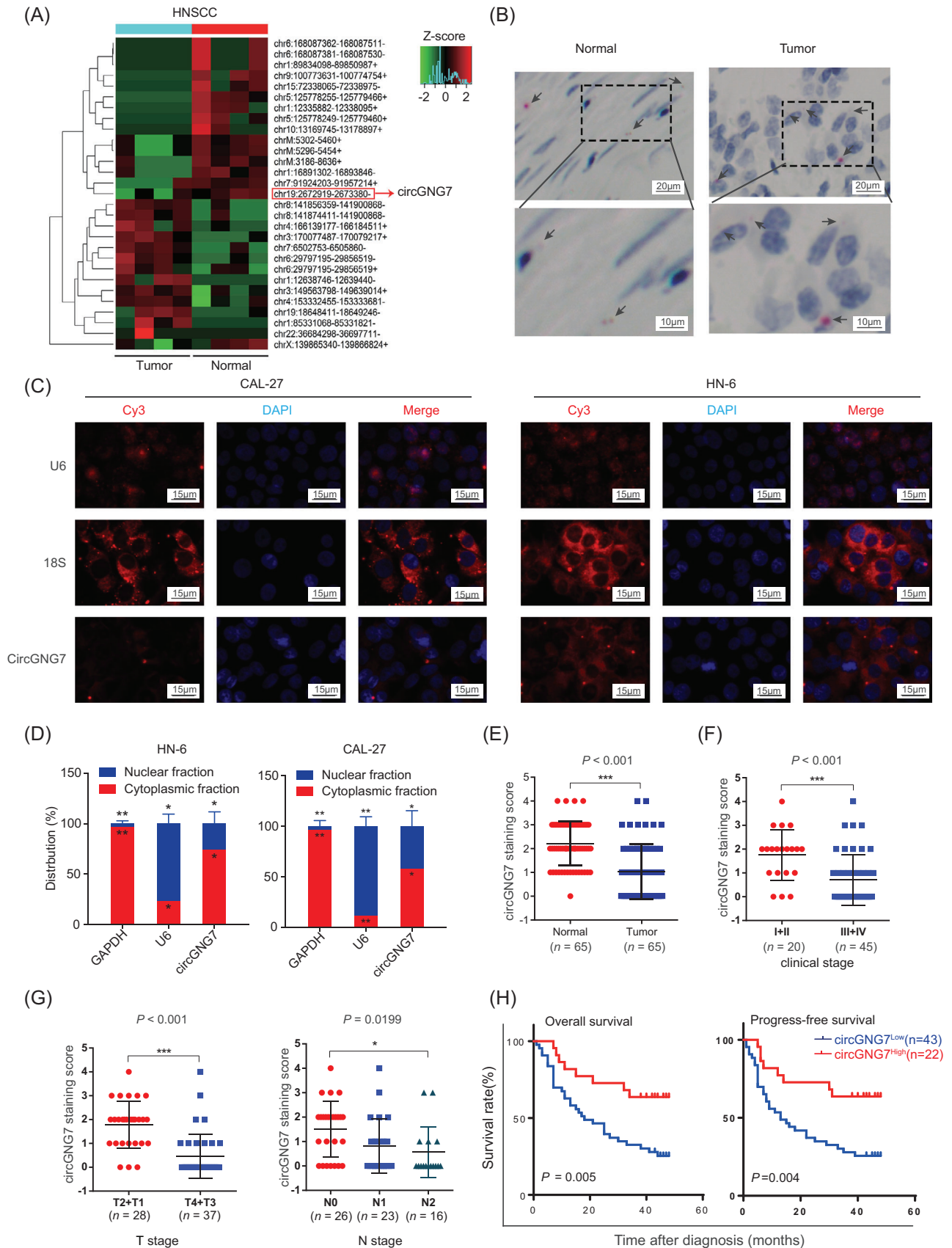
FIGURE 1 Reduced circGNG7 expression was associated with poor prognosis in HNSCC. (A) Clustered heatmap for differentially expressed circRNAs between four pairs of primary tumor tissues and adjacent normal tissues, with rows representing circRNAs and columns representing tissues. The numerical data represent the serial numbers of circRNAs in circBase. (B) The representative images of circGNG7

amplify circGNG7 from a cDNA template but not from a genomic DNA (gDNA) template, where circRNA was not present; similar results were not observed with GAPDH. Then, we used RNase R and actinomycin D (transcription inhibitor) treatment to examine the stability of circGNG7 and GNG7 in CAL27 and HN6 cells. Unlike classical circRNAs, both circGNG7 and GNG7 could be degraded by RNase R (Figure 2C). However, the half-life of circGNG7 was much longer than that of GNG7 after actinomycin D treatment (Figure 2D). In summary, these results

detected by using an RNAscope® *in situ* assay in HNSCC and adjacent normal tissues. The red dots pointed by black arrows indicate the circGNG7 blots. (C) The subcellular localization of circGNG7 was detected by FISH in CAL27 and HN6 cells. 18S RNA and U6 indicate cytoplasm and nucleus, respectively. (D) The expression level of circGNG7 in the nuclear and cytoplasm fractions was assessed by qRT-PCR in CAL27 and HN6 cells. Data are presented as mean ± SD of at least three independent experiments. (E) circGNG7 expression was detected in tumor and adjacent normal tissues from 65 HNSCC patients by RNAscope assay. (F, G) circGNG7 staining score was analyzed according to UICC stage in HNSCC patients. (H) OS and PFS of HNSCC patients were evaluated according to the circGNG7 staining score. *$P < 0.05$, **$P < 0.01$; ***$P < 0.001$. Abbreviations: circRNAs: circular RNAs; HNSCC: head and neck squamous cell carcinoma; qRT-PCR: quantitative real-time polymerase chain reaction; UICC: Union for International Cancer Control; PFS: progression-free survival; OS: overall survival
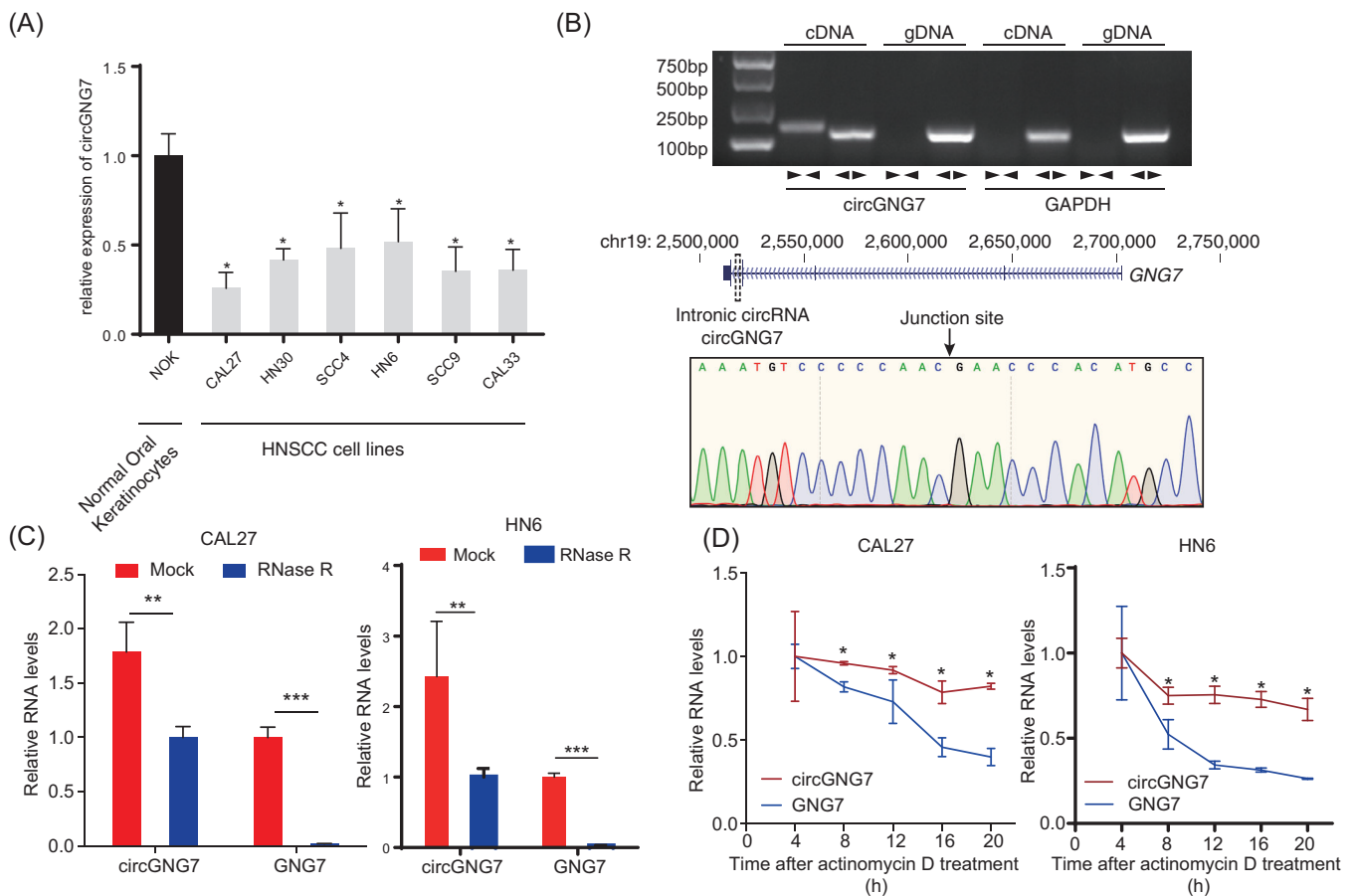
FIGURE 2 Evidence of circGNG7 as a circular RNA and its subcellular localization. (A) circGNG7 expression was measured in HNSCC cell lines and normal oral keratinocytes. (B) Schematic illustration of the origin and structure of circGNG7. The circular form of circGNG7 in cDNA and gDNA was validated by using divergent primers (◄►) and convergent primers (►◄) in CAL27 cells. GAPDH was used as a linear RNA control. The head-to-tail splicing of circGNG7 was confirmed by Sanger sequencing in CAL27 cells. (C) RNA samples were treated with RNase R to remove linear RNAs, and circGNG7 was evaluated after RNase R digestion in CAL27 and HN6 cells. For qPCR normalization, the abundance of GNG7 was calculated by standardizing over the spike DNA control and setting the PBS control. (D) RT-PCR for the abundance of circGNG7 and GNG7 in CAL27 and HN6 cells treated with actinomycin D at the indicated time points. Data are presented as mean ± SD of at least three independent experiments. *$P < 0.05$, **$P < 0.01$, ***$P < 0.001$. Abbreviations: HNSCC: head and neck squamous cell carcinoma; qPCR: quantitative real-time polymerase chain reaction; RT-PCR: reverse transcription PCR; GNG7: G protein subunit gamma 7; cDNA: complementary DNA; gDNA: genomic DNA

verified that circGNG7 was a circRNA that was distinct from canonical circRNAs.

3.3 | CircGNG7 exerted a tumor-suppressive effect in HNSCC cells

To explore the biological function of circGNG7 in HNSCC cells, we established a knockdown system using siRNAs (si-circGNG7 #1, #2, and #3) and an overexpression system using ectopic overexpression plasmids (ov-circGNG7 #1, #2, and #3). The efficacies of these reagents on circGNG7 expression were confirmed in CAL27 and HN6 cells by PCR (Supplementary Figure S3A and B). Then, we selected si-circGNG7 #2 and ov-circGNG7 #1 (with the highest efficacies) to perform further experiments. To test their effect on the host gene GNG7, we assessed GNG7 expression after knocking down or overexpressing circGNG7. Our results showed that neither knockdown nor overexpression of circGNG7 altered the expression of GNG7 (Supplementary Figure S3C and D). Using CCK-8 and colony formation assays, we found that overexpression of circGNG7 significantly inhibited the proliferation and colony formation of CAL27 and HN6 cells (Figure 3A and B), and the opposite effect was observed after circGNG7 knockdown (Supplementary Figure S3E and F). EDU is a thymine nucleoside analog and can be inserted into replicating DNA molecules during cell proliferation [21]. We observed that circGNG7 overexpression could inhibit DNA replication activity (Figure 3C) and that circGNG7 knockdown exerted the opposite effect (Supplementary Figure S3G). Then, we investigated the effect of circGNG7 on the invasion and migration of HNSCC cells. The results showed that ectopic expression of circGNG7 inhibited cell invasion and migration compared with the vector control, and silencing circGNG7 enhanced cell invasion and migration in CAL27 and HN6 cells, as shown by Transwell and wound healing assays (Figure 3D,E and Supplementary Figure S3H–J).

To verify that circGNG7 exerts similar effects *in vivo*, we established stable circGNG7-overexpressing CAL27 cells (Supplementary Figure S3K), then established a xenograft model in nude mice (Figure 3F and Supplementary Figure S3L). Both tumor volume and weight were significantly decreased in the circGNG7-overexpressing group compared with the vector control group (Figure 3G and H). In addition, the expression of Ki-67 was also decreased in the xenografts excised from the circGNG7-overexpressing group (Figure 3I). Then we established a lung metastasis model to explore the metastatic effect of circGNG7 in vivo (Figure 3J). We observed that the number of metastatic nodules was also decreased in the circGNG7-

overexpressing group compared with the vector control group (Figure 3K). In summary, circGNG7 suppressed HNSCC tumor progression.

3.4 | CircGNG7 inhibited the phosphorylation of HSP27 at Ser78 and Ser82

To determine the underlying mechanism by which circGNG7 regulates cancer cell growth, we first explored canonical ceRNA interactions between circRNAs and miRNAs. A ceRNA network was constructed to identify potential miRNAs that were associated with differentially expressed RNAs (Supplementary Table S8). Then, we verified the miRNA that was predicted to be sponged by circGNG7. To this end, we identified a possible interaction between circGNG7 and miR-34c-5p in CAL27 and HN6 cells (Figure 4A and B). However, the results from the functional assay using dual-luciferase reporters were negative (Figure 4C). Moreover, by analyzing all putative sORFs, we found that circGNG7 had no protein-coding potential (Supplementary Table S9). Thus, we hypothesized that circGNG7 might interact with functional proteins.

We performed a circGNG7 RNA pull-down assay using biotinylated DNA probes that were complementary to the circGNC7 junction sequence. This approach ensured the specificity of the biotinylated probe and that it would not pull down linear GNG7 RNAs. The precipitated proteins were silver stained and subjected to MS sequencing (Figure 5A and B). This sequencing identified a total of 92 proteins, and the majority of these targets were RNA-binding proteins (Supplementary Table S3). The top three proteins selected by peptide enrichment were chosen, and their interaction with circGNG7 was validated. These results revealed some non-specificity in alpha-2-glycoprotein 1, zinc-binding (AZGP1) and transglutaminase 3 (TGM3) binding (Figure 5C). On the other hand, HSP27, a HSP involved in the negative regulation of gastric cancer [22], showed specific binding to circGNG7 (Figure 5D).

We next determined the effects of circGNG7 on the function of HSP27. Since the activity of HSPs is largely dependent on their posttranslational modification, especially the phosphorylation of distinct sites, we altered circGNG7 expression and assessed the phosphorylation status of the HSP27 protein. We found that the phosphorylation of HSP27 at Ser78 and Ser82 was dramatically decreased, but the total HSP27 level and the phosphorylation of HSP27 at Ser15 were not affected when circGNG7 expression was upregulated in either CAL27 or HN6
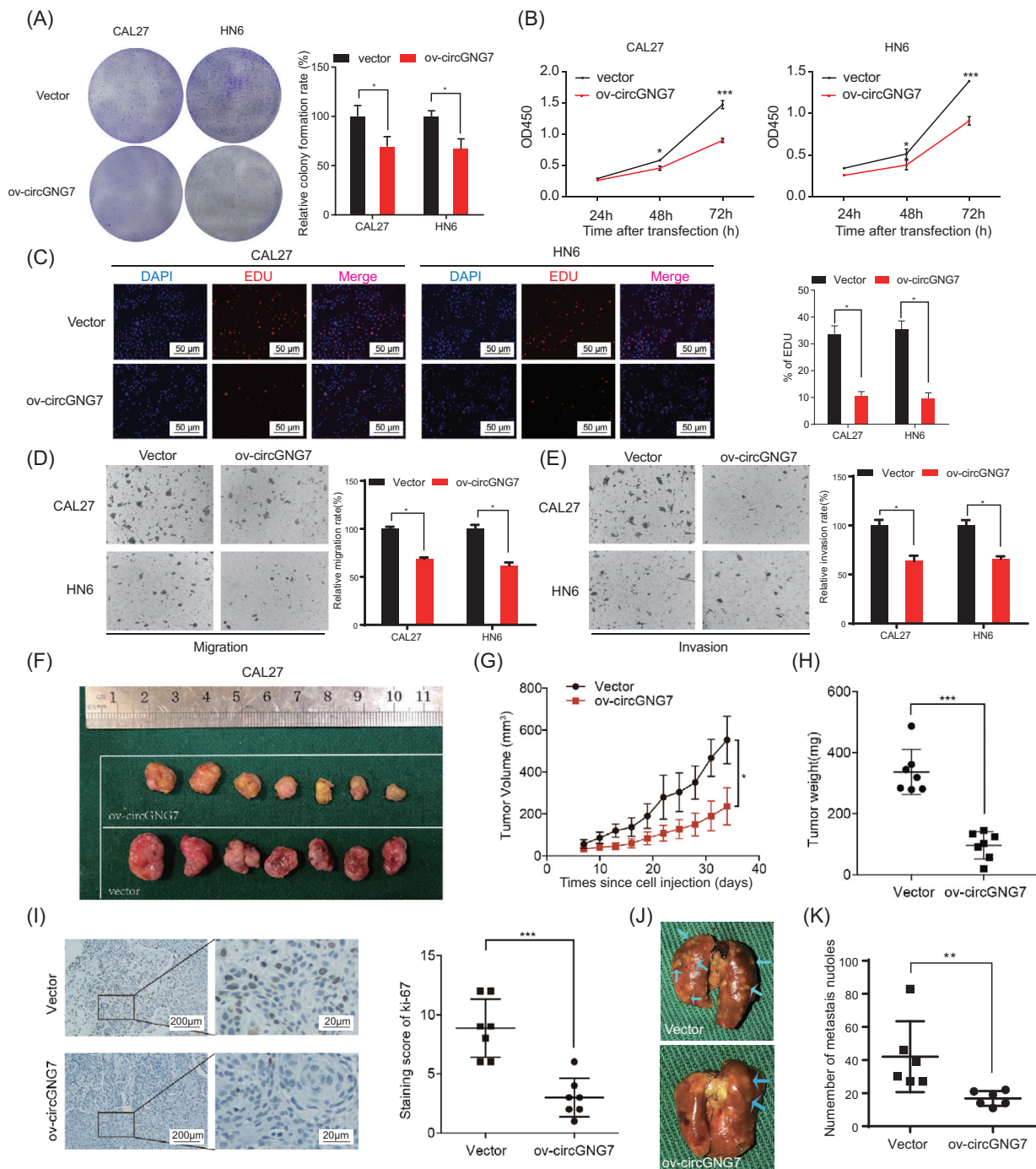
FIGURE 3 circGNG7 inhibited the progression of HNSCC cells *in vitro* and *in vivo*. HN6 and CAL27 cells were transfected with overexpression plasmid (ov-circGNG7) or vector plasmid respectively for 48 h. (A) Colony formation assays were performed. Representative images are shown, and relative colony formation rate was evaluated. (B) Cell viability after transfection was accessed by using CCK8 assays. (C) EDU assays were performed after transfection. Representative images are shown, and the proportion of EDU-positive cells was calculated. Transwell assays for cell migration (D) and invasion (E) were performed. Representative images are shown, and relative migration rate and invasion rate were calculated. (F) Representative images of xenograft tumors derived from stable circGNG7 overexpression or vector control cells are shown. (G) Primary tumor growth curves after cell injection in the stable circGNG7 overexpression or vector control groups were analyzed. (H) Tumor weight after removal from mice in the ectopic overexpression and vector control group was measured. (I) The expression of Ki-67 in xenograft tissues derived from stable circGNG7 overexpression or vector control cells was detected by immunohistochemistry. Representative images are shown, and the Ki-67 staining score was evaluated. (J) Representative images of the lungs from mice injected with stable circGNG7 overexpression or vector control cells are shown. Arrows indicate individual metastatic nodules. (K) The metastatic nodules were counted. Data are presented as mean ± SD of at least three independent experiments. *$P < 0.05$, **$P < 0.01$, ***$P < 0.001$. Abbreviations: HNSCC: head and neck squamous cell carcinoma; CCK-8: Cell Counting Kit-8; EDU: 5-ethynyl-2'-deoxyuridine
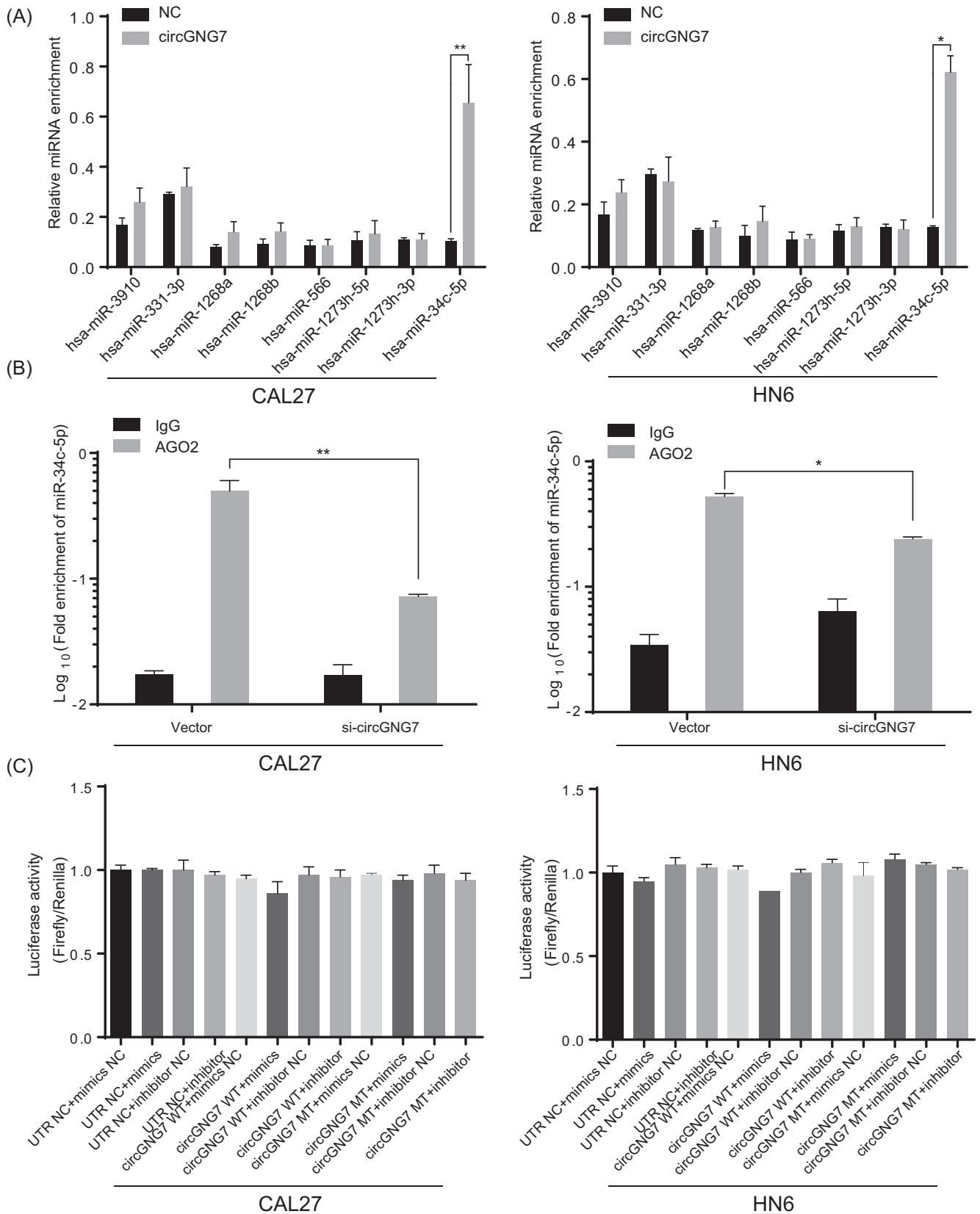
FIGURE 4 circGNG7 exerted neither miRNA interaction nor protein-coding potential in HNSCC cells. (A) The relative enrichments of miRNAs were evaluated by pull-down assay with biotinylated circGNG7 or negative control primer (NC) in CAL27 and HN6 cells. (B) The fold enrichment of miR-34c-5p and negative control was evaluated by AGO2-RIP in CAL27 and HN6 cells. (C) Dual-luciferase activities were accessed in CAL27 and HN6 cells after indicated transfection. Data are presented as mean ± SD of at least three independent experiments. *P < 0.05, **P < 0.01, ***P < 0.001. Abbreviations: AGO2-RIP: Argonaute 2-RNA immunoprecipitation; miRNAs: microRNAs.
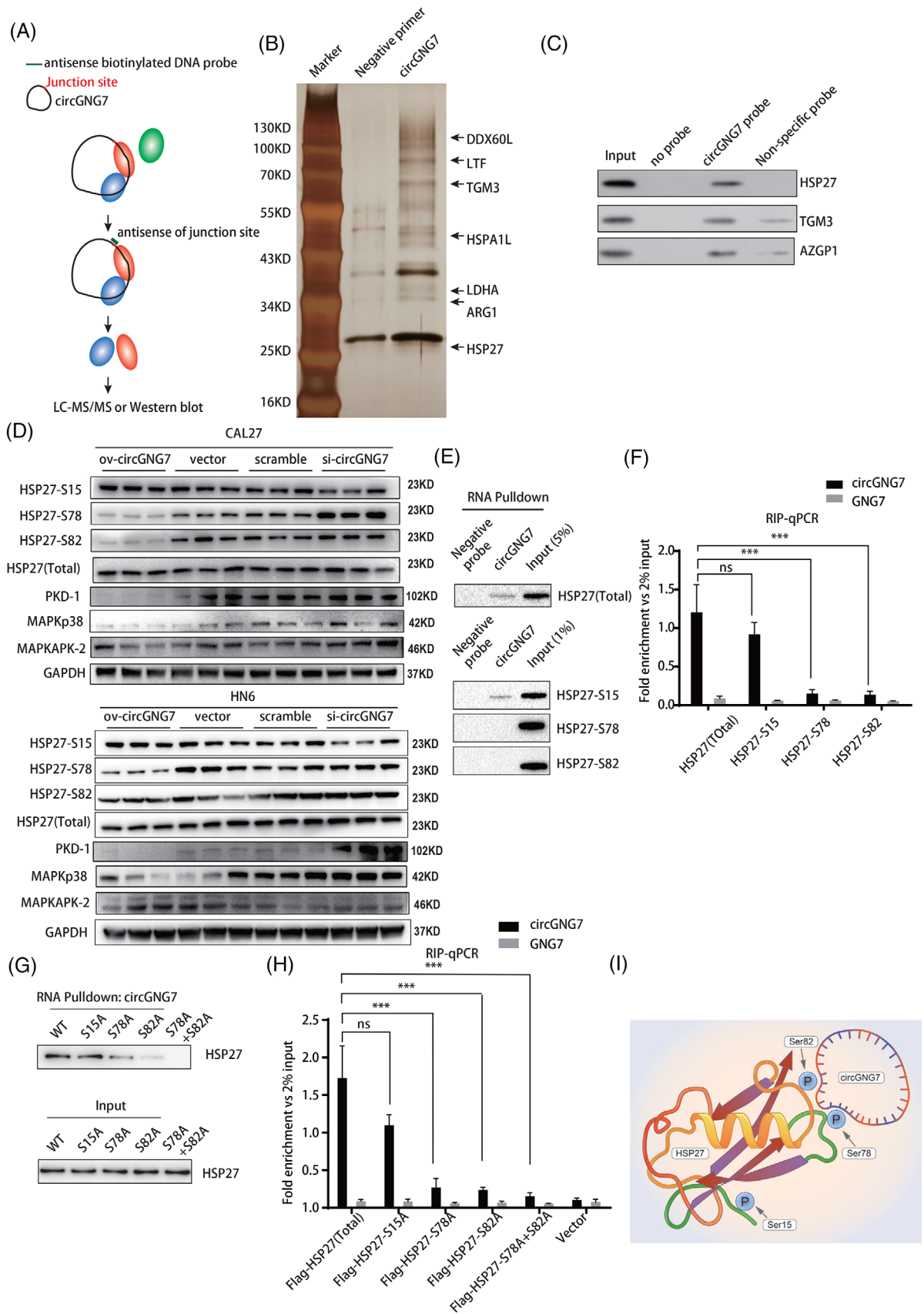
FIGURE 5 CircGNG7 inhibited the phosphorylation of HSP27 at Ser78 and Ser82. (A) Schematic diagram of the proteins binding with circGNG7. (B) CAL27 cells were transfected with circGNG7 overexpression plasmid (ov-circGNG7) or negative control plasmid. The probe-circRNA complexes were captured and subjected to proteomic analysis by LC-MS/MS system. (C) Top three enriched peptides pulled

cells. mitogen-activated protein kinase P38 (MAPKP38), MAPK-activated protein kinase-2 (MAPK-APK-2), and polycystin 1 (PKD-1) are the main upstream kinases that phosphorylate HSP27. We found that the levels of MAPKP38, MAPK-APK-2 and PKD-1 were also decreased when circGNG7 expression was upregulated. The opposite effect was observed when circGNG7 expression was downregulated (Figure 5D and Supplementary Figure S4). After transfection of CAL27 cells with a circGNG7-overexpressing plasmid, we detected the phosphorylation of HSP27 after it was pulled down with circGNG7. HSP27 was still phosphorylated at Ser15 but not at Ser78 or Ser82 (Figure 5E). Then, we examined the level of circGNG7 pulled down with phosphorylated HSP27, and the level of circGNG7 pulled down with HSP27 phosphorylated at Ser78 and Ser82 was significantly decreased, but no significant difference was observed when circGNG7 was pulled down with HSP27 phosphorylated at Ser15 (Figure 5F). These data suggest that circGNG7 could not interact with HSP27 when its Ser78 or Ser82 residues were phosphorylated. We further constructed plasmids expressing HSP27 with mutated Ser15, Ser78, and Ser82 phosphorylation sites. We found that compared with that in the WT group, the amount of HSP27 pulled down with circGNG7 in the Ser78, Ser82, and Ser78+Ser82 mutant groups was decreased, but no change was observed in the Ser15 mutant group (Figure 5G). Consistently, compared with that in the WT FLAG-HSP27 group, the amount of circGNG7 pulled down with FLAG-HSP27 proteins in the Ser78, Ser82, and Ser78+Ser82 mutant groups was significantly reduced, but no significant difference was observed in the Ser15 mutant group (Figure 5H); these results suggested that the interaction between circGNG7 and the Ser78 and Ser82 phosphorylation sites of HSP27 was weakened when the peptide structures of Ser78 and Ser82 were altered. These data indicated that circGNG7 might occupy the Ser78 and Ser82 phosphorylation sites of HSP27, but not the Ser15 phosphorylation site, and inhibit the phosphorylation of HSP27 in HNSCC cells (Figure 5I).

3.5 | CircGNG7 inhibited HNSCC progression by regulating the HSP27-JNK/P38 MAPK pathway

Previous studies have reported that HSP27 was activated by phosphorylation and its activation was associated with poor prognosis of various solid tumors, including HNSCC [23–25]. We first validated the transfection efficiency of HSP27 overexpression plasmid and siRNA in CAL27 or HN6 cells (Supplementary Figure S5A–C). Overexpression of HSP27 in CAL27 or HN6 cells could promote proliferation, migration, and invasion, and knockdown of HSP27 exerted the opposite effect (Figure 6A,B and Supplementary Figure S5D–I). We designed rescue experiments to validate the regulatory role of circGNG7 through HSP27. Overexpression of HSP27 in CAL27 or HN6 cells significantly reversed the suppressive effect of circGN7 on proliferation, invasion, and migration, whereas silencing HSP27 strengthened the suppressive effect of circGNG7 on HNSCC cells (Figure 6C,D and Supplementary Figure S5J,K). These results proved that circGNG7 inhibited the progression of HNSCC by regulating HSP27 activity.

HSP27 was previously identified as a crucial molecule in the P38 MAPK signaling pathway [26]. According to previous reports, we further validated the effect of HSP27 overexpression or silencing on the MAPK pathway. Upregulation of HSP27 expression activated P38 and c-Jun by phosphorylation in CAL27 and HN6 cells (Figure 6E). Then, we performed a rescue experiment to verify the role of circGNG7 in regulating HNSCC cells through the HSP27-JNK/P38 MAPK pathway. We observed that overexpression of HSP27 could significantly reverse the suppressive effect of circGNG7on MAPK signaling, and silencing HSP27 strengthened the suppressive effect of circGNG7 on MAPK signaling in CAL27 and HN6 cells (Figure 6E).

We further explored the effect of circGNG7 on HSP27-JNK/P38 MAPK signaling *in vivo*. Compared with the vector control, overexpression of circGNG7 in xenograft tissues led to significantly decreased levels of phosphorylated HSP27-S78 and HSP27-S82 (Figure 6F–I), and the

---

down by circGNG7 were validated by Western blotting. (D) The expression of P38, MAPK-APK-2, PKD-1 and phosphorylation level of HSP27 were detected by Western blotting in CAL27 and HN6 cells transfected with si-circGNG7, scramble, ov-circGNG7, and control vector. (E) CAL27 cells were transfected with ectopic circGNG7 plasmid. The total protein or phosphorylated protein of HSP27 pulled down by circGNG7 was accessed by Western blotting. (F) circGNG7 and GNG7 expression level pulled down by total protein or phosphorylated protein (S15, S78 and S82) of HSP27 was evaluated by qRT-PCR. (G) CAL27 cells were transfected with wild-type, mutant plasmid at phosphoacceptor site 15, 78, or 82 of HSP27 (S15A, S78A, S82A, or co-transfected with S78A and S82A. The total protein of HSP27 pulled down by circGNG7 was detected by Western blotting. (H) RIP assays were conducted to detect the expression of circGNG7 and GNG7 pulled down by total HSP27 protein, HSP27 mutant protein at phosphoacceptor site 15, 78, or 82 (S15A, S78A, S82A, or S78A and S82A) in CAL27 cells respectively. (I) Schematic diagram of the interaction between HSP27 and circGNG7. Data are presented as mean ± SD of at least three independent experiments. *$P < 0.05$, **$P < 0.01$, ***$P < 0.001$. Abbreviations: MAPK-APK-2: MAPK-activated protein kinase-2; PKD-1: polycystin 1; RT-PCR: reverse transcription polymerase chain reaction
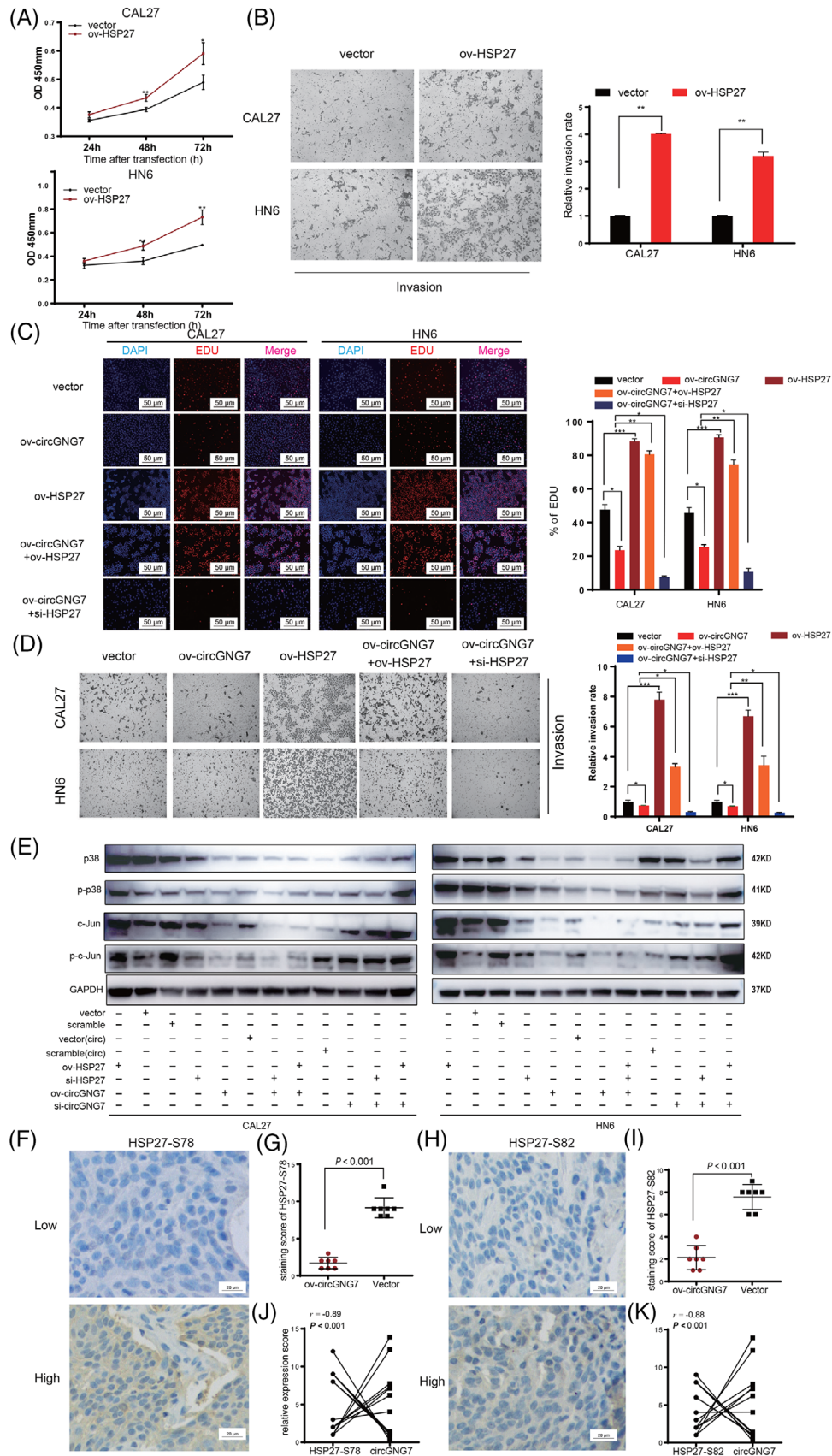
FIGURE 6 CircGNG7 inhibited HNSCC progression by regulating the HSP27-JNK/P38 MAPK pathway. HN6 and CAL27 cells were transfected with HSP27 overexpression plasmid (ov-HSP27) or vector plasmid respectively for 48 h. (A) Cell viability after transfection was accessed by using CCK8 assays in CAL27 and HN6 cells. (B) Transwell assays for cell invasion were performed. Representative images are

phosphorylated and total expression levels of c-Jun and P38 were also significantly decreased (Supplementary Figure S5L,M). These protein levels were also negatively correlated with the expression of circGNG7 (Figure 6J,K and Supplementary Figure S5N). However, the expression levels of total HSP27 and HSP27-S15 were not significantly different between the circGNG7-overexpressing and vector control groups (Supplementary Figure S5L,M), and the correlation of the expression of total HSP27 and HSP27-S15 with the expression of circGNG7 was also not significant (Supplementary Figure S5N).

3.6 | CircGNG7 expression is regulated by the binding of the transcription factor SMAD4 to the GNG7 promoter

We further investigated the factors that regulate the expression of circGNG7. Recent studies have shown that several TFs affected circRNA expression by binding to the promoter regions of their linear parental genes [27,28]. We identified 32 TFs with potential ($P < 0.001$) to bind to the GNG7 promoter (Figure 7A and Supplementary Table S10). KEGG pathway analysis was subsequently performed on this set of TFs (Supplementary Table S11). Based on the results from the KEGG pathway analysis and previously published studies about TFs in HNSCC [29–36], we knocked down the expression of 17 TFs (Supplementary Figure S6) and tested their effects on expression of circGNG7. We observed that circGNG7 expression was significantly decreased after knocking down SMAD4 expression in both the CAL27 and HN6 cell lines (Figure 7B) and that overexpression of SMAD4 led to increased expression of circGNG7 (Figure 7C). Then, we verified that SMAD4 could directly bind to the GNG7 promoter by using a ChIP assay (Figure 7D). To investigate whether SMAD4 affects circGNG7 expression, we constructed a plasmid carrying a mutant circGNG7 sequence with a defective SMAD4-binding site and transfected this mutant plasmid or the WT plasmid into CAL27 or HN6 cells. Then, we transfected a SMAD4-overexpressing plasmid or vector control into

these cells. A dual-luciferase reporter assay revealed that the luciferase activity was significantly decreased in the mutant group (Figure 7E). The results described above suggested that SMAD4 bound to the promoter region of GNG7 and affected circGNG7 expression. We further investigated the regulatory role of SMAD4 on the phosphorylation of HSP27. Our data showed that the expression of HSP27-S78 and -S82 were increased in si-SMAD4 group, and opposite effect was observed in ov-SMAD4 group (Figure 7F). The expression of HSP27-S78 and -S82 showed no difference after knocking down other 16 selected TFs (Supplementary Figure S7). Taken together, these data suggested that circGNG7 might inhibit HNSCC progression through the HSP27-JNK/P38 MAPK pathway (Figure 7G).

4 | DISCUSSION

In the current study, we first investigated and functionally studied intronic circRNAs in HNSCC. CircGNG7, an intronic circRNA identified by our whole-transcriptome sequencing, exerted strong tumor suppressive effects on HNSCC cells and was significantly associated with poor prognosis of HNSCC. Furthermore, we discovered that circGNG7, transcriptionally regulated by SMAD4, interacted with HSP27 to block the phosphorylation of Ser78 and Ser82 and subsequently inhibited HSP27-JNK/P38 MAPK oncogenic signaling in HNSCC.

The majority of circRNAs originate from a single exon or multiple exons and localize to the cytoplasm. Several intronic lariats escape degradation by debranching enzymes and exonucleases and occasionally splice into circRNAs; these molecules are called intronic circRNAs. Compared to exonic circRNAs, intronic circRNAs have rarely been investigated, and fewer than 200 intronic circRNAs have been identified to date. Intronic circRNAs are characterized by a relatively short length (average length of 280 nt), and their expression is underestimated in the present sequencing system. Zhang et al. [37] reported that several circRNAs could also be degraded by incubation with RNase R. Unlike canonical circRNAs, intronic

shown, and relative invasion rate was calculated. HN6 and CAL27 cells were transfected with vector plasmid, ov-circGNG7, ov-HSP27, ov-circGNG7+ov-HSP27, and ov-circGNG7+siHSP27 respectively for 48 h. (C) EDU assays were performed after transfection to test DNA replication activity. EDU-positive cells were counted. (D) Relative cell migration and invasion rates by transwell assays were calculated. (E) HN6 and CAL27 cells were transfected with HSP27 siRNA (si-HSP27), scrambled siRNA, ov-HSP27, vector plasmid, ov-circGNG7, vector of circRNA [vector(circ)], ov-circGNG7+ov-HSP27, ov-circGNG7+siHSP27, si-circGNG7, scramble of circRNA [scramble(circ)], si-circGNG7+ov-HSP27, and si-circGNG7+siHSP27 respectively for 48 h. The expression of c-Jun, p-c-Jun, P38, and p-P38 was evaluated by Western blotting. (F, I) Xenograft tumors were derived from stable circGNG7 overexpression or vector control cells. The expression of HSP27-S78 (F) and HSP27-S82 (I) in xenograft tissues was detected by immunohistochemistry, and representative images are shown. The staining scores of HSP27-S78 (G) and HSP27-S82 expression (J) were evaluated. The relationships between circGNG7 and HSP27-S78 (H) and HSP27-S82 (K) in xenograft tissues were analyzed. Data are presented as mean ± SD of at least three independent experiments. *$P < 0.05$, **$P < 0.01$, ***$P < 0.001$. Abbreviations: HNSCC: head and neck squamous cell carcinoma
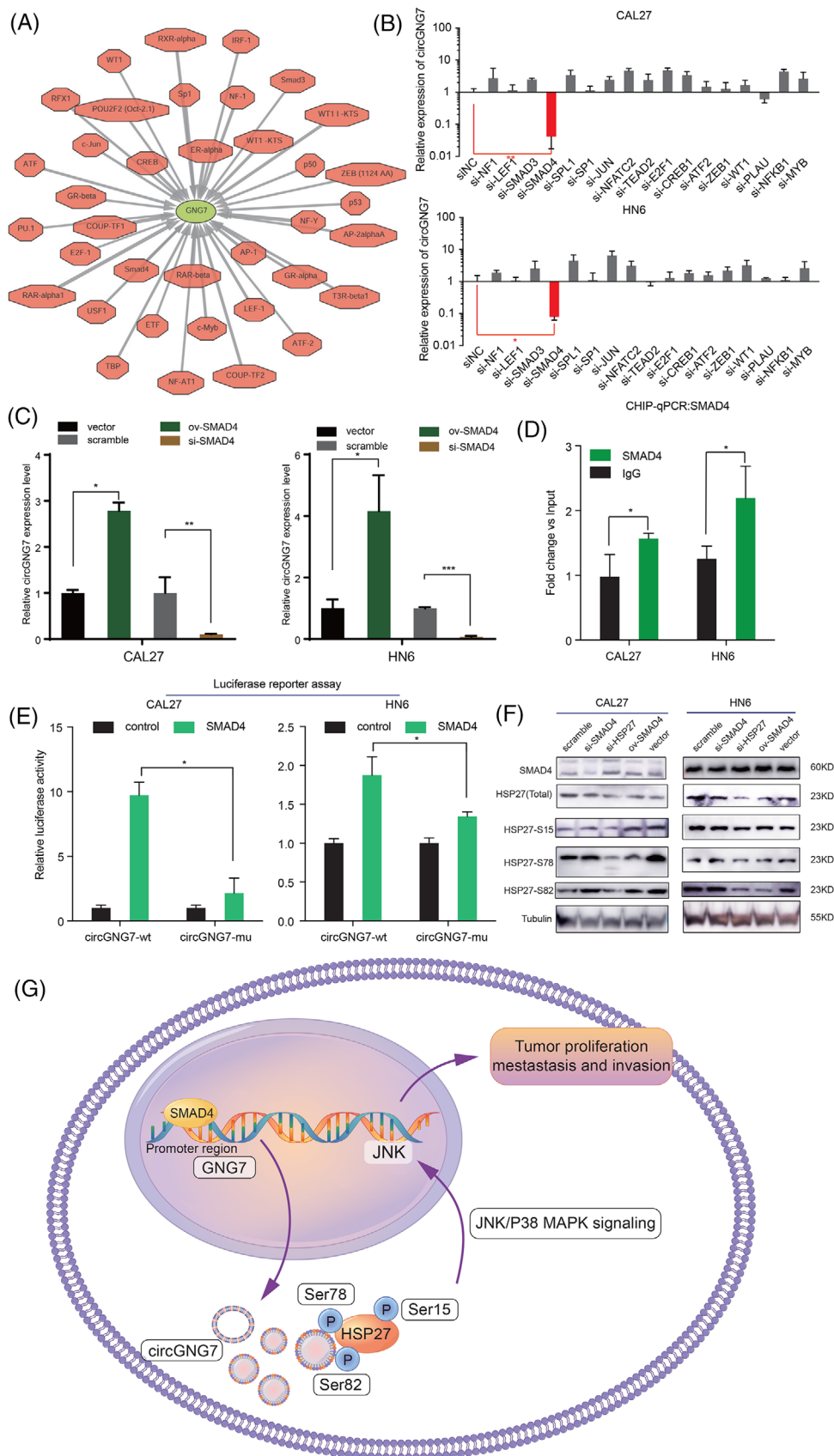
FIGURE 7 CircGNG7 expression level was regulated by SMAD4 binding on GNG7 promoter. (A) The potential transcription factors binding to GNG7 promoter were predicted by using public database LASAGNA-Search 2.0 with the threshold *P* value <0.001. (B) The circGNG7 expression was detected by RT-PCR in CAL27 and HN6 cells transfected with siRNA of selected genes (NF1, LEF1, SMAD3,

circRNAs have a 2'-5' head-tail joint that is not polyadeny-lated. intronic circRNAs are usually less stable and might be degraded by RNase R [38]. In the present study, cir-cGNGN7 was confirmed to have a circular structure by Sanger sequencing of its circular site. The sensitivity of circGNGN7 to RNase R exposure indicated potential differ-ences between intronic circRNAs and canonical circRNAs. Intronic circRNAs are currently thought to reside in the nucleus and increase the expression of their parental genes by promoting RNA polymerase II-mediated transcription or by interacting with the U1 small nuclear ribonucle-oprotein [39]. However, we discovered that circGNG7 exhibited a non-canonical subcellular localization and was mostly present in the cytoplasm. Increasing evidence has revealed that certain TFs are involved in the process of circRNA formation [40]. For example, elevated levels of the transcription factor Muscleblind (Mbl) facilitate cir-cMbl formation by binding to its flanking introns [41]. Our data suggested that the transcription factor SMAD4 was able to bind to a fragment of the GNG7 promoter and that aberrantly expressed SMAD4 enhanced circGNG7 expres-sion. However, the mechanism underlying the ectopic distribution of circGNG7 requires further investigation.

Although our previous study discovered that cir-cGNG7 expression was reduced in metastatic oral mucosal melanoma patients and that this reduced expression was closely associated with poor prognosis [18], circGNG7 was not annotated in the reported HNSCC circRNA dataset. In the present study, circGNG7 expression was reduced both in HNSCC tissue and cell lines, and this decreased expres-sion was associated with poor clinical outcome. Therefore, we further analyzed the biological function of circGNG7 in HNSCC cell lines and in a nude mouse model, and we revealed that elevated circGNG7 expression significantly inhibited the progression of HNSCC and that decreased circGNG7 expression had the opposite effect. These find-ings increased the understanding of circGNG7 biogene-sis and expanded the spectrum of functional circRNAs in HNSCC.

In general, circRNAs regulate cancer cells via three mechanisms. In addition to competing with miRNAs to bind to mRNAs, distinct circRNAs interact with functional proteins, and some have protein-coding potential [4]. Stud-ies have reported that circRNAs can interact with and enhance the function of the polymerase II complex [5]. In addition, a few circRNAs act as protein scaffolds, facilitat-ing the colocalization of enzymes, such as phosphatases, acetylases, and ubiquitin ligases [5]. Several circRNAs can recruit specific proteins to certain loci or subcellular com-partments and may also function as sponges or decoys of RNA-binding proteins and indirectly regulate their func-tions [42–44]. However, the detailed binding sites and how circRNAs alter the expression and function of the pro-teins to which they bind remain unknown. In the current study, we investigated whether circGNG7 could bind to ser-ine residues 78 and 82 of the functional protein HSP27, occupying these phosphorylation sites and thus inhibiting the phosphorylation of HSP27 in malignant signaling cas-cades.

HSP27 (also named HSPB1) is a member of the super-family of small HSPs, and it functions as an ATP-independent molecular chaperone by forming a complex with its homologous protein HSP25 [45]. The sequence of HSP27 contains 10.2% serine residues, and Ser15, Ser78, and Ser82 are currently known to be phosphoacceptor sites [45]. The aberrant phosphorylation of HSP27 in human cancers (including HNSCC) is closely related to aggressive tumor behavior, drug resistance, and poor disease prog-nosis [46]. However, the phosphorylation state of each serine residue does not coincide with the biogenesis of cancer. Increased phosphorylation of HSP27 at Ser78 was observed in HER-2/neu-positive breast cancer patients, and an inhibitor of P38 MAPK reduced the phosphoryla-tion of HSP27 at Ser78, while the phosphorylation of Ser15 and Ser82 was barely affected [47]. The protein kinase p90 ribosomal S6 kinase 2 (RSK2) physically binds to HSP27 and was also reported to enhance its phosphorylation at Ser78 and Ser82 but not at Ser15 in HNSCC [48]. HSP27 is directly phosphorylated at Ser15, Ser78, and Ser82 by the P38 kinase substrate MAPK-APK-2, and PKD-1 can phos-phorylate HSP27 at Ser82 in a P38 signaling-independent manner [49]. In the present study, we found that the levels

---

SMAD4, SPL1, SP1, JUN, NFATC2, TEAD2, E2F1, CREB1, ATF2, ZEB1, WT1, PLAU, NFKB1, and MYB) for 24 h. (C-D) CAL27 and HN6 cells were transfected with SMAD4 overexpression plasmid (ov-SMAD4) or vector for 48 h. (C) The circGNG7 expression was evaluated by RT-PCR. (D) The binding of SMAD4 at the GNG7 promoter region was detected by a chromatin immunoprecipitation assay. (E) CAL27 and HN6 cells were co-transfected with circGNG7 mutant/wildtype plasmid and ov-SMAD4, and the luciferase activity was determined by using a dual luciferase reporter assay after 24 h. (F) The expression levels of SMAD4, total HSP27, HSP27-S15, HSP27-S78, and HSP27-S82 were evaluated by Western blotting in CAL27 and HN6 cells transfected with si-SMAD4, si-HSP27, scramble, ov-SMAD4, and vector for 24 h. (G) Schematic diagram of the regulation of circGNG7 by SMAD4 binding with serine residues 78, and 82, occupying the phosphorylation site of functional protein HSP27, hindering the phosphorylation of HSP27, which reduces the HSP27-JNK/P38 MAPK oncogenic signaling and inhibits HNSCC progression. Data are presented as mean ± SD of at least three independent experiments. *$P < 0.05$, **$P < 0.01$, ***$P < 0.001$. Abbreviations: RT-PCR: reverse transcription polymerase chain reaction

of P38, MAPK-APK-2, and PKD-1 were decreased in the ov-circGNG7 group, suggesting that circGNG7 could inhibit HSP27 phosphorylation. We also found that circGNG7 did not change the expression level of HSP27 but blocked the Ser78 and Ser82 phosphorylation sites, not the Ser15 phosphorylation site, thereby inhibiting the function of HSP27. These findings indicated a novel regulatory mechanism of circRNAs.

HSP27 is a crucial effector in cancer development because it interacts with multiple downstream molecules. Studies have shown that HSP27 is involved in the activation of MAPK signaling [26,50,51]. In our GO and KEGG pathway analyses of the whole-transcriptome sequencing, we showed that cirGNG7 might regulate cancer-related pathways, such as Ras signaling, PI3K-Akt signaling, and chemokine signaling pathways, and the MAPK pathway is downstream of the Ras signaling pathway. MAPK signaling is divided into the canonical MAPK pathway, the JNK/P38 MAPK pathway, and the signal-regulated kinase 5 (ERK5) MAPK pathway (known as the MEK5/ERK5 pathway) [52]. Consistently, our data showed that HSP27 could phosphorylate P38 and c-Jun, which are canonical downstream effector proteins in the MAPK pathway, indicating that the phosphorylation of HSP27 activated JNK/P38 MAPK signaling and subsequently promoted HNSCC progression.

5 | CONCLUSIONS

In summary, we verified that circGNG7 played a robust role in suppressing the tumorigenesis of HNSCC. Different from the traditional understanding, circGNG7 was primarily distributed in the cytoplasm, and its expression could be upregulated by the transcription factor SMAD4. CircGNG7 blocked the Ser78 and Ser82 phosphorylation sites, but not the Ser15 phosphorylation site, of HSP27, thus inhibiting the phosphorylation of HSP27 in HNSCC cells. Furthermore, this study showed that reduced HSP27 phosphorylation inactivated downstream proteins, including P38 and c-Jun, to inhibit the progression of HNSCC. These results established that circGNG7 may have prognostic and therapeutic applications in HNSCC patients.

AUTHOR CONTRIBUTIONS
GR, JH and XZ financially supported the research. JH and MR collected the HNSCC tissues and conducted validation assays. XZ performed statistical analysis. WG independently supervised the results to control data quality. DW and ZL performed functional experiments. HJ conducted all the molecular mechanism experiments and wrote the manuscript. ZH performed the in vivo experiments.

ETHICS APPROVAL AND CONSENT TO PARTICIPATE
Our study was approved by Ethics Board of the Shanghai Ninth People's Hospital, and informed consent was provided by the enrolled patients.

DATA AVAILABILITY STATEMENT
The circRNA expression analysis used during the current study is accessible through GEO series accession number GSE159382 (https://www.ncbi.nlm.nih.gov/geo/query/acc.cgi?acc=GSE159382).

CONFLICT OF INTEREST
The authors declare that they have no competing interests.

ORCID
Wei Guo https://orcid.org/0000-0003-1946-8765
Guoxin Ren https://orcid.org/0000-0003-0231-4938

REFERENCES
1. Siegel RL, Miller KD, Jemal A. Cancer statistics, 2019. CA Cancer J Clin. 2019; 69: 7-34.
2. Lau A, Yang WF, Li KY, Su YX. Systemic therapy in recurrent or metastatic head and neck squamous cell carcinoma- a systematic review and meta-analysis. Crit Rev Oncol Hematol. 2020; 153: 102984.
3. Marur S, Forastiere AA. Head and neck squamous cell carcinoma: update on epidemiology, diagnosis, and treatment. Mayo Clin Proc. 2016; 91: 386-396.
4. Li J, Sun D, Pu W, Wang J, Peng Y. Circular RNAs in cancer: biogenesis, function, and clinical significance. Trends Cancer. 2020; 6: 319-336.
5. Xiao MS, Ai Y, Wilusz JE. Biogenesis and functions of circular RNAs come into focus. Trends Cell Biol. 2020; 30: 226-240.
6. Liu L, Wang J, Khanabdali R, Kalionis B, Tai X, Xia S. Circular RNAs: isolation, characterization and their potential role in diseases. RNA Biol. 2017; 14: 1715-1721.
7. Ng WL, Mohd Mohidin TB, Shukla K. Functional role of circular RNAs in cancer development and progression. RNA Biol. 2018; 15: 995-1005.
8. Lei M, Zheng G, Ning Q, Zheng J, Dong D. Translation and functional roles of circular RNAs in human cancer. Mol Cancer. 2020; 19: 30.
9. Verduci L, Ferraiuolo M, Sacconi A, Ganci F, Vitale J, Colombo T, et al. The oncogenic role of circPVT1 in head and neck squamous cell carcinoma is mediated through

the mutant p53/YAP/TEAD transcription-competent complex. Genome Biol. 2017; 18: 237.

10. Wu Y, Zhang Y, Zheng X, Dai F, Lu Y, Dai L, et al. Circular RNA circCORO1C promotes laryngeal squamous cell carcinoma progression by modulating the let-7c-5p/PBX3 axis. Mol Cancer. 2020; 19: 99.

11. Zhang J, Hu H, Zhao Y, Zhao Y. CDR1as is overexpressed in laryngeal squamous cell carcinoma to promote the tumour's progression via miR-7 signals. Cell Prolif. 2018; 51: e12521.

12. Zhao W, Cui Y, Liu L, Qi X, Liu J, Ma S, et al. Splicing factor derived circular RNA circUHRF1 accelerates oral squamous cell carcinoma tumorigenesis via feedback loop. Cell Death Differ. 2020; 27: 919-933.

13. Huang SH, O'Sullivan B. Overview of the 8th Edition TNM classification for head and neck cancer. Curr Treat Options Oncol. 2017; 18: 40.

14. Ball CA, Awad IA, Demeter J, Gollub J, Hebert JM, Hernandez-Boussard T, et al. The Stanford Microarray Database accommodates additional microarray platforms and data formats. Nucleic Acids Res. 2005; 33: D580-582.

15. Ju H, Hu Z, Lu Y, Wu Y, Zhang L, Wei D, et al. TLR4 activation leads to anti-EGFR therapy resistance in head and neck squamous cell carcinoma. Am J Cancer Res. 2020; 10: 454-472.

16. Wang F, Flanagan J, Su N, Wang LC, Bui S, Nielson A, et al. RNAscope: a novel in situ RNA analysis platform for formalin-fixed, paraffin-embedded tissues. J Mol Diagn. 2012; 14: 22-29.

17. Guo JC, Fang SS, Wu Y, Zhang JH, Chen Y, Liu J, et al. CNIT: a fast and accurate web tool for identifying protein-coding and long non-coding transcripts based on intrinsic sequence composition. Nucleic Acids Res. 2019; 47: W516-W522.

18. Zhou LY, Zhai M, Huang Y, Xu S, An T, Wang YH, et al. The circular RNA ACR attenuates myocardial ischemia/reperfusion injury by suppressing autophagy via modulation of the Pink1/FAM65B pathway. Cell Death Differ. 2019; 26: 1299-1315.

19. Ju H, Zhang L, Mao L, Liu S, Xia W, Hu J, et al. Altered expression pattern of circular RNAs in metastatic oral mucosal melanoma. Am J Cancer Res. 2018; 8: 1788-1800.

20. Hartmann S, Szaumkessel M, Salaverria I, Simon R, Sauter G, Kiwerska K, et al. Loss of protein expression and recurrent DNA hypermethylation of the GNG7 gene in squamous cell carcinoma of the head and neck. J Appl Genet. 2012; 53: 167-174.

21. Sismour AM, Benner SA. The use of thymidine analogs to improve the replication of an extra DNA base pair: a synthetic biological system. Nucleic Acids Res. 2005; 33: 5640-5646.

22. Shi DB, Ma RR, Zhang H, Hou F, Guo XY, Gao P. GAGE7B promotes tumor metastasis and growth via activating the p38delta/pMAPKAPK2/pHSP27 pathway in gastric cancer. J Exp Clin Cancer Res. 2019; 38: 124.

23. Zheng G, Zhang Z, Liu H, Xiong Y, Luo L, Jia X, et al. HSP27-mediated extracellular and intracellular signaling pathways synergistically confer chemoresistance in squamous cell carcinoma of tongue. Clin Cancer Res. 2018; 24: 1163-1175.

24. Paladino L, Vitale AM, Santonocito R, Pitruzzella A, Cipolla C, Graceffa G, et al. Molecular chaperones and thyroid cancer. Int J Mol Sci. 2021; 22(8):4196.

25. Spigel DR, Shipley DL, Waterhouse DM, Jones SF, Ward PJ, Shih KC, et al. A randomized, double-blinded, phase II trial of carboplatin and pemetrexed with or without Apatorsen (OGX-427) in patients with previously untreated stage IV Non-squamous-

non-small-cell lung cancer: the SPRUCE trial. Oncologist. 2019; 24: e1409-e1416.

26. James J, Srivastava A, Valuparampil Varghese M, Eccles CA, Zemskova M, Rafikova O, et al. Heme induces rapid endothelial barrier dysfunction via the MKK3/p38MAPK axis. Blood. 2020; 136(6):749-754.

27. Wu J, Jiang Z, Chen C, Hu Q, Fu Z, Chen J, et al. CircIRAK3 sponges miR-3607 to facilitate breast cancer metastasis. Cancer Lett. 2018; 430: 179-192.

28. Zhang X, Xu Y, Qian Z, Zheng W, Wu Q, Chen Y, et al. circRNA_104075 stimulates YAP-dependent tumorigenesis through the regulation of HNF4a and may serve as a diagnostic marker in hepatocellular carcinoma. Cell Death Dis. 2018; 9: 1091.

29. Cancer Genome Atlas, N. Comprehensive genomic characterization of head and neck squamous cell carcinomas. Nature 2015; 517: 576-582.

30. Chen X, Liu L, Mims J, Punska EC, Williams KE, Zhao W, et al. Analysis of DNA methylation and gene expression in radiation-resistant head and neck tumors. Epigenetics. 2015; 10: 545-561.

31. Citron F, Armenia J, Franchin G, Polesel J, Talamini R, D'Andrea S, et al. An integrated approach identifies mediators of local recurrence in head and neck squamous carcinoma. Clin Cancer Res. 2017; 23: 3769-3780.

32. Ilmarinen T, Munne P, Hagstrom J, Haglund C, Auvinen E, Virtanen EI, et al. Prevalence of high-risk human papillomavirus infection and cancer gene mutations in nonmalignant tonsils. Oral Oncol. 2017; 73: 77-82.

33. Park Y, Kim W, Lee JM, Park J, Cho JK, Pang K, et al. Cytoplasmic DRAK1 overexpressed in head and neck cancers inhibits TGF-beta1 tumor suppressor activity by binding to Smad3 to interrupt its complex formation with Smad4. Oncogene. 2015; 34: 5037-5045.

34. Scanlon CS, Van Tubergen EA, Inglehart RC, D'Silva NJ. Biomarkers of epithelial-mesenchymal transition in squamous cell carcinoma. J Dent Res. 2013; 92: 114-121.

35. Sun S, Wu Y, Guo W, Yu F, Kong L, Ren Y, et al. STAT3/HOTAIR signaling axis regulates HNSCC growth in an EZH2-dependent manner. Clin Cancer Res. 2018; 24: 2665-2677.

36. Zhang H, Zhu Z, Meadows GG. Chronic alcohol consumption impairs distribution and compromises circulation of B cells in B16BL6 melanoma-bearing mice. J Immunol. 2012; 189: 1340-1348.

37. Zhang Y, Yang L, Chen LL. Characterization of circular RNAs. Methods Mol Biol. 2016; 1402:215-227.

38. Mumtaz PT, Taban Q, Dar MA, Mir S, Haq ZU, Zargar SM, et al. Deep insights in circular RNAs: from biogenesis to therapeutics. Biol Proced Online. 2020; 22:10.

39. Kristensen LS, Andersen MS, Stagsted LVW, Ebbesen KK, Hansen TB, Kjems J. The biogenesis, biology and characterization of circular RNAs. Nat Rev Genet. 2019; 20: 675-691.

40. Li X, Yang L, Chen LL. The biogenesis, functions, and challenges of circular RNAs. Mol Cell. 2018; 71: 428-442.

41. Ashwal-Fluss R, Meyer M, Pamudurti NR, Ivanov A, Bartok O, Hanan M, et al. circRNA biogenesis competes with pre-mRNA splicing. Mol Cell. 2014; 56: 55-66.

42. Chen N, Zhao G, Yan X, Lv Z, Yin H, Zhang S, et al. A novel FLI1 exonic circular RNA promotes metastasis in breast cancer by

coordinately regulating TET1 and DNMT1. Genome Biol. 2018; 19: 218.

43. Hanniford D, Ulloa-Morales A, Karz A, Berzoti-Coelho MG, Moubarak RS, Sanchez-Sendra B, et al. Epigenetic silencing of CDR1as drives IGF2BP3-mediated melanoma invasion and metastasis. Cancer Cell. 2020; 37: 55-70 e15.

44. Nan A, Chen L, Zhang N, Jia Y, Li X, Zhou H, et al. Circular RNA circNOL10 inhibits lung cancer development by promoting SCLM1-mediated transcriptional regulation of the humanin polypeptide family. Adv Sci (Weinh). 2019; 6: 1800654.

45. Kostenko S, Moens U. Heat shock protein 27 phosphorylation: kinases, phosphatases, functions and pathology. Cell Mol Life Sci 2009; 66: 3289-3307.

46. Wu J, Liu T, Rios Z, Mei Q, Lin X, Cao S. Heat shock proteins and cancer. Trends Pharmacol Sci. 2017; 38: 226-256.

47. Zhang D, Wong LL, Koay ES. Phosphorylation of Ser78 of Hsp27 correlated with HER-2/neu status and lymph node positivity in breast cancer. Mol Cancer. 2007; 6: 52.

48. Kang S, Elf S, Lythgoe K, Hitosugi T, Taunton J, Zhou W, et al. p90 ribosomal S6 kinase 2 promotes invasion and metastasis of human head and neck squamous cell carcinoma cells. J Clin Invest. 2010; 120: 1165-1177.

49. Evans IM, Britton G, Zachary IC. Vascular endothelial growth factor induces heat shock protein (HSP) 27 serine 82 phosphorylation and endothelial tubulogenesis via protein kinase D and independent of p38 kinase. Cell Signal. 2008; 20: 1375-1384.

50. Deng K, Liu L, Tan X, Zhang Z, Li J, Ou Y, et al. WIP1 promotes cancer stem cell properties by inhibiting p38 MAPK in NSCLC. Signal Transduct Target Ther. 2020; 5: 36.

51. Zoubeidi A, Zardan A, Wiedmann RM, Locke J, Beraldi E, Fazli L, et al. Hsp27 promotes insulin-like growth factor-I survival signaling in prostate cancer via p90Rsk-dependent phosphorylation and inactivation of BAD. Cancer Res. 2010; 70: 2307-2317.

52. Lei YY, Wang WJ, Mei JH, Wang CL. Mitogen-activated protein kinase signal transduction in solid tumors. Asian Pac J Cancer Prev. 2014;15(20):8539-8548.

SUPPORTING INFORMATION

Additional supporting information may be found in the online version of the article at the publisher's website.